BMC Medical Imaging

RESEARCH

Open Access

Dual-phase contrast-enhanced CT-based intratumoral and peritumoral radiomics for preoperative prediction of lymphovascular invasion in gastric cancer

Yun-hui Zhou[1], Yang Liu[1], Xin Zhang[2], Hong Pu[1†] and Hang Li[1*†]

Abstract

Background To develop and validate a dual-phase contrast-enhanced computed tomography (CT)-based intratumoral and peritumoral radiomics for the prediction of lymphovascular invasion (LVI) in patients with gastric cancer.

Method Three hundred and eighty-three patients with gastric cancer (training cohort, 269 patients; test cohort, 114 patients) were retrospectively enrolled between January 2017 and June 2023. Radiomics features were extracted from the intratumoral volume (ITV) and peritumoral volume (PTV) on CT images at arterial phase (AP) and venous phase (VP), and selected by the least absolute shrinkage and selection operator. Radiomics models were constructed by logistic regression. The clinical-radiomics combined model incorporating the most predictive radiomics signature and clinical risk factors were developed with multivariate analysis. Receiver operating characteristic (ROC) curves were used to evaluate the prediction performance of models.

Results Clinical model comprised of three clinical risk factors including tumor differentiation, CT-reported lymph node metastasis status and CT-TNM staging showed good performance with an area under the ROC curve (AUC) of 0.804 and 0.825 in the training and test cohort, respectively. Compared with the other radiomics models, dual-phase (AP + VP) CT-based ITV + PTV radiomics model presented superior AUC of 0.844 and 0.835 in the training and test cohort, respectively. Clinical-radiomics combined model further improved the discriminatory performance (AUC, 0.903) in the training and test cohort (AUC, 0.901). Decision curve analysis confirmed the net benefit of clinical-radiomics combined model. Subgroup analyses showed that the clinical-radiomics nomogram showed the best performance with an AUC of 0.879 and 0.883 for predicting LVI in T1-T2 and T3-T4 gastric cancer compared with the clinical model and the ITV + PTV-AP + VP radiomics model, respectively.

†Hong Pu and Hang Li contributed equally to this work.

*Correspondence:
Hang Li
lihang111222@126.com

Full list of author information is available at the end of the article

Conclusions Clinical-radiomics combined model integrating clinical risk factors and dual-phase contrast-enhanced CT-based intratumoral and peritumoral radiomics signatures provided favorable performance for predicting LVI in gastric cancer.

Keywords Lymphovascular invasion, Gastric cancer, CT, Nomograms

Introduction

Gastric cancer is the fifth most common malignant neoplasms, and it ranks the third leading cause of cancer-related deaths globally [1, 2]. Surgical resection remains the main treatment option for resectable gastric cancer, with additional therapy methods used as supplements when necessary. There is an urgent need for a solution to the problem of post-operative tumor recurrence and metastasis that affect the prognosis of the patients with gastric cancer. Although TNM staging guidelines could be used to obtain reliable prognostic indications, it has been noted that assessment of the prognosis of patients with gastric cancer based on TNM staging alone is not always satisfactory. Lymphovascular invasion (LVI) is defined as the presence of tumor thrombi in the vascular and/or lymphatic wall infiltration or the presence of tumor emboli with an endothelial-lined space. LVI in gastric cancer is an independent risk factor for patient prognosis, especially in advanced cancers with lymph node metastases (LNM) [3–5]. Even patients with early gastric cancer with LVI positive had a higher rate of recurrence and a lower overall survival rate of 3–5 years than those with a negative LVI status [6]. Therefore, these studies suggested that the preoperative prediction of LVI can be helpful in facilitating risk stratification and change the strategy regarding the use of adjuvant therapy for high-risk patients [3, 7]. However, LVI is mainly determined by postoperative tumor pathology specimen detection, and the preoperative prediction of LVI is remains difficult.

Some studies have focused on preoperative prediction of LVI using contrast-enhanced computed tomography (CT). Ma et al. reported that CT attenuation difference of tumor on multiphasic dynamic CT images is associated with LVI, but repeatability measurement of inter-observer has not determined [8]. Previous studies showed CT-based radiomics of gastric cancer could predict lymph node metastasis, tumor Lauren classification, perineural invasion and response to neoadjuvant therapy and showed favorable performance [9–12]. A recently study focused on prediction of LVI by combining dual-phase CT-based radiomics and clinical factors, and showed the moderate discriminatory performance [13]. However, most of these studies only focused on intratumoral regions, while peritumoral regions, which may have important information about the tumor, were excluded [14]. Tumor heterogeneity exists not only in cancer cells but also in nonmalignant cells and infiltrating cells around the tumor, usually referred to as the peritumoral microenvironment. To our knowledge, there are few studies on the prediction of LVI based on intratumoral and peritumoral radiomics of dual-phase contrast-enhanced CT images. Therefore, the purpose of this study is to develop and validate a dual-phase contrast-enhanced CT-based intratumoral and peritumoral radiomics for preoperative prediction of LVI in gastric cancer.

Materials and methods

Patients

This study was approved by the institutional review board and requirement to obtain written informed consent was waived because of the retrospective nature of the study. 472 patients with gastric cancer between January 2017 and June 2023 were retrospectively enrolled in this study. The median time between the diagnosis and surgery was 7 days (range, 3–45 days). All the patients underwent follow-up after surgery and were evaluated at 3 months intervals in the first year and 6-month intervals for the next 2-years. Thereafter, annual review was performed. CT scans and/or endoscopically were determined to identify recurrence and metastasis. The inclusion criteria consisted of (a) pathologically confirmed primary gastric adenocarcinoma; (b) performing radical tumor resection; (c) undergoing enhanced CT examination within one month prior to surgical resection; and (d) without other synchronous malignant tumors. Among the 472 patients, 89 patients were excluded for the following reasons: (a) receive neoadjuvant treatment prior to surgery ($n = 55$); (b) poor image quality due to severe artifacts and distortion ($n = 10$) (c) the maximal diameter of tumor is less than 6 mm, insufficient to place a valid volume of interest (VOI) ($n = 24$). The remaining 383 patients (275 men, 108 women; mean age, 63.0 ± 11.3years) were finally enrolled in this study (Fig. 1). The whole cohort was randomly stratified into training and test cohort at the ratio of 7:3.

Imaging protocol

The 383 patients underwent contrast-enhanced 256-section spiral CT (SOMATOM Force CT and GE Revolution CT). The patients were advised to fast from solid food for at least 8 h and drink 600–1000 ml water in two hours prior to CT examination. The acquisition parameters for contrast enhanced CT were as follows: 120 kV tube voltage, automated tube current, reconstruction section thickness of 3 mm, matrix 512 × 512. Iohexol (Omnipaque, GE Healthcare, 350 mg iodine/ml) was injected

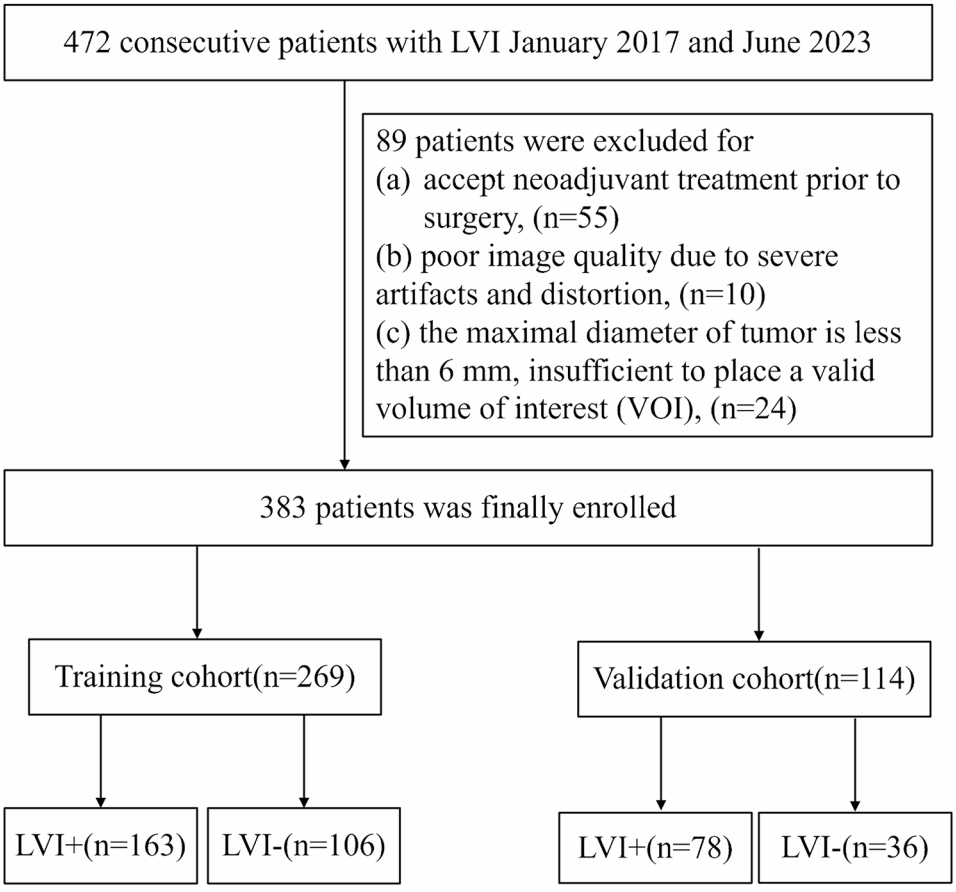

Fig. 1 Flowchart of patient selection

into the cubital vein at a dose of 1.2–1.5 mL/kg and at a rate of 2-3mL/s. Intelligent triggering technology determined the time of arterial phase (AP) scanning. The AP scan was triggered by an automatic threshold (120 HU), and the venous phase (VP) image acquisition was performed after a 30s delay.

Clinical feature

The clinical factors included the age, gender, tumor location, CA19-9 level and carcinoembryonic antigen (CEA) level. All patients underwent radical resection of the tumor. The subjective CT features were independently evaluated and recorded by two radiologists (the first and last author, with 3 and 10 years of experience in abdominal imaging, respectively), who were blinded to the histopathology and the clinical history. If the results were inconsistent, they were resolved by consultation. Subjective CT features were evaluated as follows: thickness of the tumor, measured at the maximal thickness of the tumor on transverse CT imaging; maximum diameter of tumor, measured at the tumor's largest cross-sectional area on transverse CT imaging; T-staging, defined as the depth of primary tumor infiltrating into the gastric wall [15]; CT- LNM, if the short-axis diameter was larger than 6 mm for perigastric LN and larger than 8 mm for extraperigastric LN [16].

Clinical factors and subjective CT features were analyzed by the univariate and multivariate logistic regression analysis in the training cohort. The area under the receiver operating characteristic (ROC) curve (AUC) was calculated to evaluate the performance of the clinical model in the training and test cohort.

Histologic analysis

Preoperative tumor differentiation was evaluated by endoscopic biopsy according to the WHO classification of tumors of the digestive system [17]. Postoperative histopathological specimens were analyzed by two pathologists. If the results were inconsistent, they were resolved by consultation. LVI defined as the presence of tumor thrombi in the vascular and/or lymphatic wall infiltration or the presence of tumor emboli with an endothelial-lined space. The diagnosis of LVI was classified according to the 8th American Joint Committee on Cancer Staging (AJCC) system [18]: V0, V1, V2 indicate no venous invasion, microscopic venous invasion, and macroscopic venous invasion, respectively. L0 and L1 indicate lymphatic invasion negative and lymphatic invasion positive,

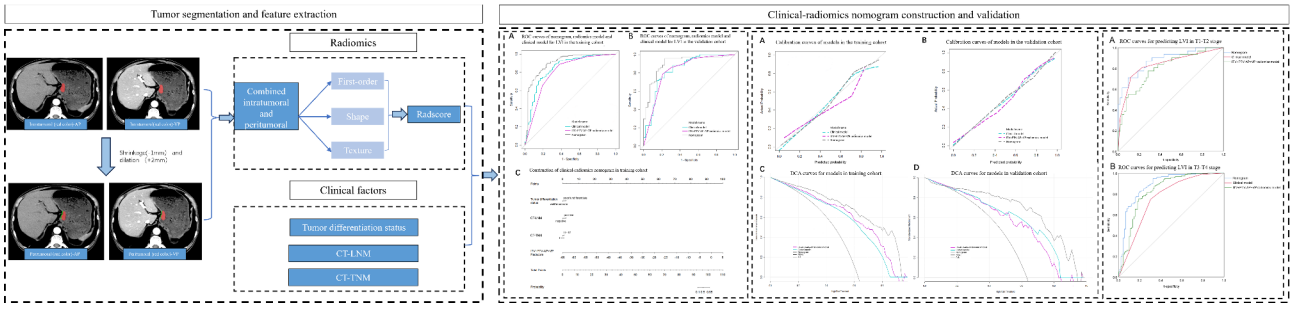

Fig. 2 The workflow of a typical radiomics process in our study

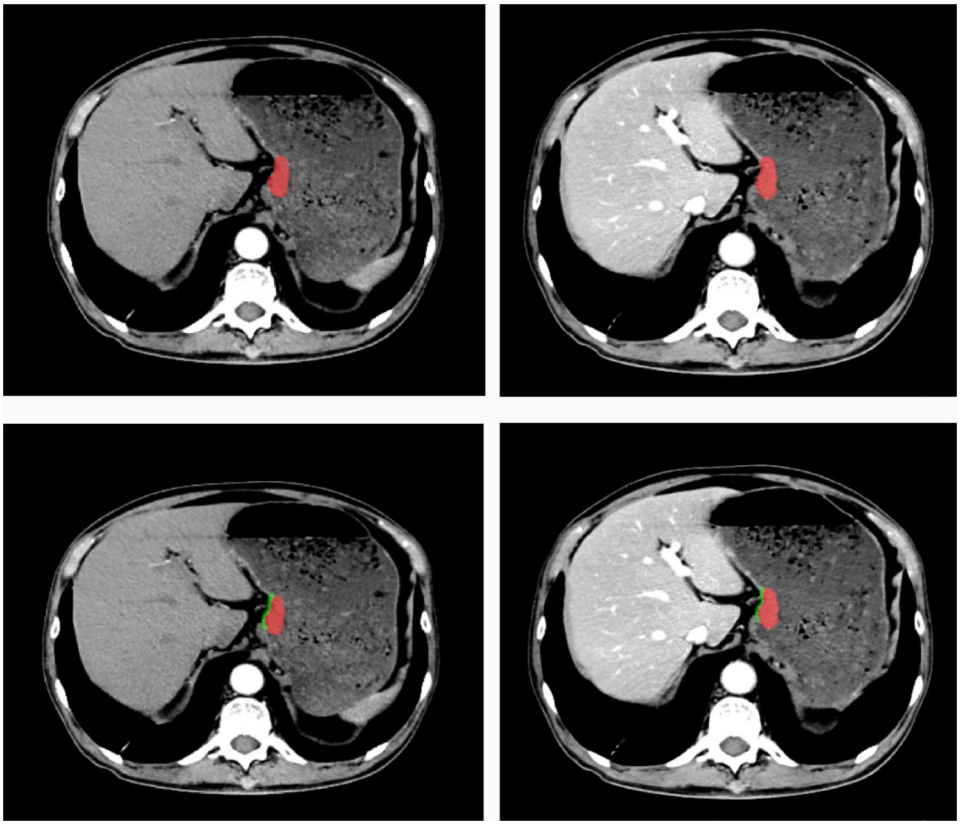

Fig. 3 Lesion segmentation of a typical gastric cancer on dual-phase contrast-enhanced CT images

respectively. L0 and V0 were defined as LVI negative while V1-2 and L1 were defined as LVI positive.

Tumor segmentation

A flowchart of radiomics process is shown in Fig. 2. Tumor delineation was performed on the entire three-dimensional tumor volume on CT images by the first radiologist (the first author) using ITK-SNAP software (www.itksnap.org). A manually defined region of interest (ROI) was firstly delineated to cover the whole tumor area on CT images at VP, and then applied to CT images at AP with slight adjustment to acquire the tailored ROIs. For the segmentation of peritumoral regions, the manual delineations were similar to the original study [12]. An example of lesion segmentation is shown in Fig. 3. Blood vessels and air are avoided as much as possible.

Thirty patients' data were randomly selected for assessing interobserver and intraobserver agreement of features extraction by intraclass correlation coefficient (ICC) analysis. Features with ICC coefficients greater than 0.8, indicating good stability and reliability, were retained for further analysis.

Radiomics feature selection and radiomics model construction

A total of 1037 radiomics features, including first-order features of 18 intensity statistics and 14 3D shape features, 24 Gy-level co-occurrence matrix (GLCM), 16 Gy-level

size zone matrix (GLSZM), 16 Gy-level run length matrix (GLRLM), 5 neighboring gray-tone difference matrix (NGTDM), and 14 Gy-level dependence matrix (GLDM) features and features with two filters, and 744 wavelet features and 186 LoG filtered features with a sigma of 2.0 and 3.0. R software (version 3.5.1), were extracted from intratumoral and peritumoral regions. The maximum relevance and minimum redundancy were first performed to select the top 20 radiomics features. The least absolute shrinkage and selection operator (LASSO) regression was further used to select radiomics features. Finally, the optimized subset of features was obtained using multiple logistic regression. Selected features were weighted by their respective coefficients to construct a radiomics signature. The most predictive radiomics signature score (radscore) was selected by AUC value for the subsequent analysis.

The nomogram construction and evaluation

The most predictive radiomics signatures, clinical factors, and subjective CT features were used to establish the clinical-radiomics combined model. A nomogram was generated for predicting LVI. ROC curves were generated to assess the discriminatory ability. Decision curve analysis (DCA) was used to evaluate clinical utility of the nomogram. A calibration curve was generated to calibrate the nomogram.

Statistical analysis

Statistical analyses were performed at SPSS (version 23.0) and R software. The relationship between clinical baseline characteristics and LVI was evaluated by Chi-squared test, independent two-sample t test, and Fisher's exact test (where appropriate). ROC analysis was carried out to evaluate the model discrimination performance. The predictive performance of the nomogram was evaluated by Calibration plots. DCA was used to evaluate the clinical usefulness of the nomograms. The differences of AUCs between the models were compared using Delong's test.

Results

Patient characteristics

Among the 383 patients (mean age, 63.0 years; range 21–88 years), 269 patients were in the training cohort (163 LVI + and 106LVI -) and 114 patients were in the test cohort (78 LVI + and 36 LVI-). The rates of LVI + were 60.59% (163/269) and 68.42% (78/114) in the training and test cohorts, respectively. Significant differences were found in tumor size, depth of invasion, CT-reported lymph node status, CT-TNM staging, and differentiation status between LVI + and LVI- in the training cohort and test cohort (all $P < 0.05$). There were no significant differences in the age, tumor location, the level of CA19-9 and CEA between LVI + and LVI- in both cohorts (all $P > 0.05$). The characteristics of the patients between LVI + and LVI- in both cohorts were given in Table 1.

Feature selection, development, and test of radiomics models

A total of 6, 3, 6, 1, 6, 5, and 5 radiomics features were selected to construct ITV-AP, PTV-AP, ITV-VP, PTV-VP, ITV + PTV-AP, ITV + PTV-VP, and ITV + PTV-AP + VP radiomics signature, respectively. The final formula of the Radscore used to predict LVI is shown in Table 2. Among all the radiomics models, combining ITV and PTV at dual-phase CT-based radiomics model (ITV + PTV-AP + VP radiomics model) resulted in the highest capability for predicting LVI, with AUCs of 0.844(95%CI: 0.792–0.896) and 0.835 (95%CI: 0.756–0.915) in the training cohort and test cohort, respectively. Multivariate logistic regression analysis revealed that LVI was independently predicted by ITV + PTV-AP + VP radscore, differentiation status, CT-reported lymph node metastasis status, and CT-TNM staging (Table 3). Therefore, a nomogram was constructed by adding the ITV + PTV-AP + VP radscore [odds ratio (OR) = 2.95] to the clinical factors [differentiation status (OR = 0.3)] and subjective CT features [CT-reported lymph node metastasis status (OR = 5.06) and CT-TNM staging (OR = 2.67)]. The establishment of the clinical-radiomics nomogram and a summary of the performance for each model were shown in Fig. 4**and** Table 4. Compared with the clinical model, the clinical-radiomics combined model provided a higher AUC in the training cohort (0.903 vs. 0.804, $p = 0.06$) and test cohort (0.901 vs. 0.825, $p = 0.2$). Compared with the ITV + PTV-AP + VP radiomics model, the clinical-radiomics combined model provided a higher AUC in the training cohort (0.903 vs. 0.844, $p = 0.003$) and test cohort (0.901 vs. 0.835, $p = 0.02$).

Clinical utility

The calibration curve showed that the three models fit well in both the training cohort and the test cohort, among which the combined clinical-radiomics nomogram was the best (Fig. 5). The result of the DCA indicated that the nomogram had more benefit than the other models for predicting LVI when the threshold probability ranged from 0.15 to 0.95 in the training cohort and from 0.22 to 0.95 in the test cohort (Fig. 5).

Subgroup analyses

Subgroup analyses of the nomogram, clinical model and radiomics model are shown in Tables 5**and** Fig. 6. There were 31 LVI + patients and 53 LVI- patients at the T1-2 stage. The clinical-radiomics nomogram showed higher AUC than that of clinical model (0.879 vs. 0.837, $p = 0.265$) and ITV + PTV-AP + VP radiomics model (0.879 vs. 0.803, $p = 0.054$) for predicting LVI + at the

Table 1 Clinical factors and subjective CT features of patients

Characteristics	Training cohort($n=269$)			Test cohort($n=114$)		
	LVI-($n=106$)	LVI+($n=163$)	*P*	LVI-($n=36$)	LVI+($n=78$)	*P*
Age(year)	62.9 ± 11.6	62.4 ± 11.6	0.737	65.6(10.8)	63.6(10.9)	0.348
Sex			0.022			0.955
Male	69(65.1%)	128(78.5%)		24(66.7%)	54(69.2%)	
Female	37(34.9%)	35(21.5%)		12(33.3%)	24(30.8%)	
Tumor location			0.059			0.853
upper 1/3	23(21.7%)	23(14.1%)		6(16.7%)	12(15.4%)	
middle 1/3	22(20.6%)	30(18.4%)		7(19.4%)	16(20.5%)	
lower 1/3	50(47.2%)	74(45.4%)		14(38.9%)	25(32.1%)	
≥ 2/3	11(10.4%)	36(22.1%)		9(25.0%)	25(32.1%)	
Tumor size (mm)	43.3 ± 23.7	55.5 ± 27.2	< 0.001	50.2 ± 19.1	62.3 ± 21.8	0.004
Tumor thickness (mm)	15.7 ± 6.28	18.1 ± 6.37	0.002	17.3(7.18)	18.7(7.22)	0.346
CT-Depth of invasion			< 0.001			0.008
T1~T2	42(39.6%)	24(14.7%)		11(30.6%)	7(8.97%)	
T3~T4	64(60.4%)	139(85.3%)		25(69.4%)	71(91.0%)	
CT-LNM			< 0.001			< 0.001
Negative	54(50.9%)	16(9.8%)		19(52.8%)	2(2.56%)	
Positive	52(49.1%)	147(90.2%)		17(47.2%)	76(97.4%)	
CT-Tumor stage			< 0.001			< 0.001
I~II	70(66.0%)	39(23.9%)		26(72.2%)	13(16.7%)	
III~IV	36(34.0%)	124(76.1%)		10(27.8%)	65(83.3%)	
Differentiation			< 0.001			< 0.001
Poor/undifferentiated	55(51.9%)	138(84.7%)		19(52.8%)	68(87.2%)	
Well/moderate	51(48.1%)	25(15.3%)		17(47.2%)	10(12.8%)	
CA19-9			1			0.919
Normal (≤ 5.0 mg/ml)	85(80.2%)	130(79.8%)		31(86.1%)	65(83.3%)	
Elevated (>5.0 mg/ml)	21(19.8%)	33(20.2%)		5(13.9%)	13(16.7%)	
CEA			0.850			0.128
Normal (≤ 37.0u/ml)	88(83.0%)	138(84.7%)		32(88.9%)	58(74.4%)	
Elevated (>37.0u/ml)	18(17.0%)	25(15.3%)		4(11.1%)	20(25.6%)	

Data are number of patients (%) or *p* value; *P* values were obtained with the chi-square test, and a *p* value < 0.05 indicates a significant difference in patients' clinicopathological characteristics between cases with positive LVI and cases with negative LVI;

LVI: lymphovascular invasion; CT: Computed Tomography; LNM: lymph node metastasis; CEA: carcinoembryonic antigen; CA19-9: carbohydrate antigen 19 – 9;

T1-2 stage. Both the clinical-radiomics nomogram and ITV + PTV-AP + VP radiomics model achieved higher sensitivity (1.000 vs. 0.903) than that of clinical model at the T1-2 stage. There were 210 patients with LVI + and 89 patients with LVI- at the T3-4 stage. The clinical-radiomics nomogram showed higher AUC than that of clinical model (0.883 vs. 0.756, $p<0.001$) and ITV + PTV-AP + VP radiomics model (0.883 vs. 0.828, $p<0.001$) for predicting LVI + at the T3-4 stage.

Discussion

In this study, we developed and validated several radiomics models, clinical model and clinical-radiomics nomogram for prediction of LVI in gastric cancer. We found that the clinical-radiomics nomogram showed the best performance than the other models for predicting LVI in gastric cancer with the AUC of 0.903 and 0.901 in the training cohort and test cohort, respectively. For subgroup analyses, our results showed clinical-radiomics nomogram also showed best performance with AUC of 0.879 and 0.883 for predicting LVI in T1-T2 and T3-T4 gastric cancer, respectively.

Several previous studies have shown that CT-based radiomics could be used to predict LVI in gastric cancer [19–21]. Consistent with these findings, our results showed that intratumoral radiomics model could predict LVI in gastric cancer with moderate diagnostic performance. Fan et al. reported that radiomics model integrating PET/CT (first-order and GLCM) and enhanced CT radiomics features (Shape, first-order, GLDM, and GLSZM) achieved AUC of 0.849 [20]. We also found some of the similar radiomics features such as first-order and GLDM in intratumoral radiomics model. It should be noted that PET/CT is not a routine tool for preoperative assessing gastric cancer. Several studies also showed enhanced CT radiomics features derived from intratumoral region could predict LVI (AUC, 0.603–0.785) [13, 22–24]. However, these previous studies were essentially

Table 2 Radiomics signature score formula of different models in the training cohort

VarName	Formula
ITV-AP radiomics model	Radscore = -2.413*wavelet.HHH_gldm_Low Gray Level Emphasis+-1.953*wavelet.HHL_gldm_Gray Level Variance+-1.469*wavelet.HLH_glcm_Cluster Tendency + 1.692*wavelet.HHL_glcm_Difference Average + 0.799*wavelet.HLH_first order_Median + 1.121*wavelet.HHH_ngtdm_Complexity+-2.437*wavelet.HLL_glcm_Idm + 1.5*wavelet.HHL_glcm_Contrast + 0.718
PTV-AP radiomics model	Radscore = 0.483*original_shape_Minor Axis Length+-0.33*log.sigma.2.0.mm.3D_gldm_Small Dependence Low Gray Level Emphasis + 0.401*wavelet.LHH_glszm_Small Area Low Gray Level Emphasis + 0.664
ITV-VP radiomics model	Radscore = 21.127*wavelet.HHH_gldm_Small Dependence High Gray Level Emphasis+-11.605*wavelet.HHH_glcm_Sum Squares+-3.413*wavelet.HHH_glcm_Maximum Probability + 3.894*wavelet.HHH_glcm_Idn + 1.843*wavelet.HLL_gldm_Small Dependence Emphasis+-11.803*wavelet.LLL_glcm_Maximum Probability + -0.265
PTV-VP radiomics model	Radscore = 0.483*original_shape_Minor Axis Length+-0.33* original_shape_Minor Axis Length + 0.401* original_shape_Minor Axis Length + 0.664
ITV + PTV-AP radiomics model	Radscore = -3.176* ITV_AP_ wavelet.HHH_gldm_Low Gray Level Emphasis + 1.788* ITV_AP_ original_glcm_Idm+-3.273* ITV_AP_ wavelet.LLL_glcm_Maximum Probability + 2.275* ITV_AP_ wavelet.HHH_ngtdm_Complexity + 1.453* ITV_AP_ wavelet.HHL_glcm_Contrast+-5.613* ITV_AP_ wavelet.LHH_glrlm_Short Run Emphasis + 0.347
ITV + PTV-VP radiomics model	Radscore = 0.428*ITV_VP_wavelet.HLL_glszm_Size Zone NonUniformity+-0.216*ITV_VP_original_gldm_Small Dependence Low Gray Level Emphasis+-0.33*ITV_VP_wavelet.HLL_glcm_Cluster Shade + 0.702*PTV_VP_wavelet.HHH_glcm_Cluster Prominence+-2.445*ITV_VP_wavelet.HHL_glszm_Small Area Low Gray Level Emphasis + 0.389
ITV + PTV-AP + VP radiomics model	Radscore = 0.347*PTV_VP_original_shape_Elongation + 0.768*ITV_AP_wavelet.HLL_glcm_Correlation+-3.555*ITV_AP_wavelet.HLL_glrlm_Low Gray Level Run Emphasis + 0.619*PTV_VP_original_shape_Minor Axis Length+-3.064*ITV_AP_wavelet.HLH_glszm_Zone% + 0.217
Clinical model	Model = -0.816-1.21*Differentation + 1.622*CT-LNM + 0.982*CT-TNM staging
Nomogram	Model = -0.861-1.343*Differentation + 1.364*CT-LNM + 0.649*CT-TNM staging + 0.898*ITV + PTV-AP + VP Radscore

CI: confidence intervals; AUC: the area under the receiver operating characteristic curve; ITV: intratumoral volume; PTV: peritumoral volume; AP: arterial phase; VP: venous phase

Table 3 Univariate and multivariate logistic regression analysis for clinical characteristics and radiomics signature score in the training cohort

Parameters	Univariate analysis		*P*	Multivariate analysis		*P*
	OR	95%CI		OR	95%CI	
Gender	0.94	0.52,1.70	0.844			
Age	0.99	0.97,1.01	0.391			
CEA	0.89	0.46,1.72	0.719			
CA19-9	1.07	0.55,2.08	0.991			
Tumor Differentation	0.20	0.11,0.35	<0.001	0.30	0.16,0.57	< 0.001
CT-TNM staging	7.47	4.29,13.04	<0.001	2.67	1.30,5.49	0.009
CT-LNM	11.91	6.15,23.06	<0.001	5.06	2.22,11.54	< 0.001
CT-Depth of invasion	4.25	2.39,7.57	<0.001			
Tumor location	1.34	1.03,1.74	0.031			
Tumor thickness	1.07	1.02,1.12	0.003			
Tumor maximum diameter	1.02	1.01,1.04	<0.001			
ITV + PTV-AP + VP radscore	2.95	2.16,4.03	<0.001	2.46	1.78,3.38	<0.001

CEA: carcinoembryonic antigen; CA19-9: carbohydrate antigen 19 – 9; CT: Computed Tomography; TNM: Tumor Node Metastasis; LNM: lymph node metastasis; Radscore: radiomics score; OR: odds ratio

based on intratumoral radiomics features. Some studies have shown that the peritumoral region still carried some relevant information about primary tumor in gastric cancer [25, 26]. Thus, we selected and integrated different intratumoral and/or peritumoral radiomics features and constructed model. In this study, we also found similar radiomics features with these previous studies, such as GLCM, GLDM, GLRLM, and GLSZM. Moreover, our study also showed other useful radiomics feature such as Shape from peritumoral region instead of intratumoral region. In the peritumoral radiomics features, Shape features, particularly the Minor Axis Length, were of paramount importance. This feature indicated tumor growth patterns and boundaries in relation to surrounding tissues, indirectly reflecting tumor infiltrative behavior. Although peritumoral radiomics model had lower performance than that of intratumoral radiomics model for predicting LVI (AUC, 0.626 vs. 0.789 for AP; 0.638 vs. 0.750 for VP), adding it to intratumoral radiomics features further improved the predictive ability (AUC, 0.794 for VP) in the validation group. This finding was consistent with Liu et al. who also confirmed peritumoral radiomics model had lower performance than that of intratumoral radiomics model for predicting pathological

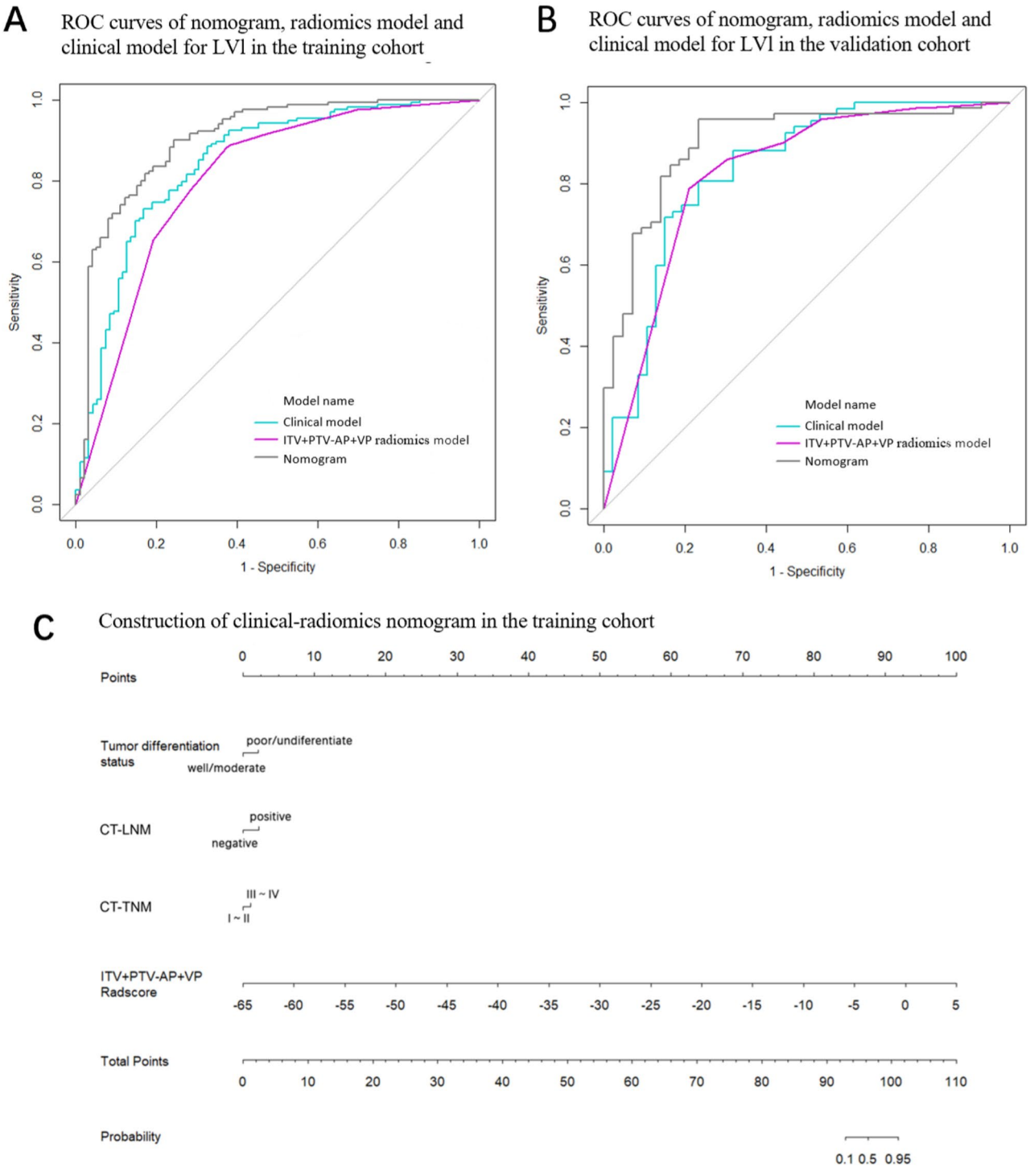

Fig. 4 Receiver operating characteristic curves of radiomics model, clinical model and clinical-radiomics nomogram for predicting lymphovascular invasion (LVI) of rectal cancer in the training cohort (**A**) and test cohort (**B**). The predictive nomogram of LVI(**C**)

responses after neoadjuvant chemotherapy in advanced gastric cancer [27]. Despite Yardımcı et al. [28] indicated that intratumoral enhanced CT radiomics model using Random Forest algorithms achieved good performance (AUC, 0.894), there were only 68 patients in the study, which may result in overfitting. The detailed comparison of radiomics models is shown in Table S1.

Moreover, by establishing combined radiomics models derived from both intratumoral and peritumoral radiomics features on AP and VP, we could achieve a

Table 4 Prediction performance of different models in the training cohort and test cohort

Data set	Model	AUC(95%CI)	Accuracy (%)	Specificity (%)	Sensitivity (%)
Training cohort	ITV-AP radiomics model	0.827(0.770–0.884)	0.833	0.660	0.935
	PTV-AP radiomics model	0.677(0.612–0.743)	0.602	0.800	0.494
	ITV-VP radiomics model	0.755(0.694–0.817)	0.758	0.515	0.905
	PTV-VP radiomics model	0.652(0.586–0.718)	0.632	0.653	0.620
	ITV + PTV-AP radiomics model	0.827(0.770–0.884)	0.833	0.660	0.935
	ITV + PTV-VP radiomics model	0.800(0.742–0.857)	0.729	0.785	0.699
	ITV + PTV-AP + VP radiomics model	0.844(0.792–0.896)	0.766	0.832	0.730
	Clinical model	0.804(0.749–0.859)	0.788	0.626	0.882
	Nomogram	0.903(0.863–0.943)	0.848	0.758	0.900
Test cohort	ITV-AP radiomics model	0.789(0.689–0.890)	0.807	0.500	0.986
	PTV-AP radiomics model	0.626(0.524–0.728)	0.605	0.766	0.493
	ITV-VP radiomics model	0.750(0.653–0.848)	0.754	0.585	0.849
	PTV-VP radiomics model	0.638(0.536–0.741)	0.623	0.591	0.643
	ITV + PTV-AP radiomics model	0.789(0.689–0.890)	0.807	0.500	0.986
	ITV + PTV-VP radiomics model	0.794(0.708–0.880)	0.711	0.633	0.769
	ITV + PTV-AP + VP model	0.835(0.756–0.915)	0.763	0.851	0.701
	Clinical model	0.825(0.747–0.903)	0.772	0.558	0.901
	Nomogram	0.901(0.841–0.962)	0.886	0.767	0.958

CI: confidence intervals; AUC: the area under the receiver operating characteristic curve; ITV: intratumoral volume; PTV: peritumoral volume; AP: arterial phase; VP: venous phase

more comprehensive understanding of tumor complexity. Our finding showed that the ITV + PTV-AP + VP radiomics model performed better than the other radiomics models, with the AUCs of 0.844 and 0.835 in the training and test cohort, respectively. The ITV + PTV-AP + VP radiomics model included five radiomics features, as Elongation, Minor Axis Length, Correlation, Low Gray Level Run Emphasis, Zone%. The first two shape features were extracted from peritumoral region, and the other features were extracted from intratumoral region. Low Gray Level Run Emphasis and Zone% were the two main features that showed stabler and better classification capability for the LVI in gastric cancer. The negative coefficient of the two features could discriminate the heterogeneous texture distribution, implying notable tumor heterogeneity. This result indicated the role of the intratumoral and peritumoral regions for the prediction of LVI in the gastric cancer.

However, when combining the intratumoral and peritumoral radiomics features of dual phase contrast-enhanced CT, the role of PTV-AP radscore seemed to be not enough important for the prediction of LVI. The possible explanation could be as follow: Lymphangiogenesis and angiogenesis are mainly distributed in the area around the tumor, and subjected to the tumor cells' replication compression, the lymphatic vessels in the intratumoral areas shrink, collapse, shut, and become nonfunctional [29]. At the same time, the lymphatic vessels in the peritumoral areas or at the tumor marginal area are often enlarged and dilated [30, 31]. Most advanced gastric cancers with good enhancement gradually experience significant transmural enhancement from the arterial phase to the portal vein phase [32, 33]. Most of the tumor lesions present as bilayers in the arterial phase, with a moderately enhanced inner layer and a mildly enhanced outer layer. With the extension of the scanning time, the enhancement of the outer layer of the tumor increased and gradually converged with the enhancement of the inner region [34]. Compared with the arterial phase, the portal vein phase may reflect more functional angiogenesis of the tumor and represent the distribution of contrast agents in the space. Therefore, peritumoral area of tumor in the venous phase may provide more useful information for evaluating LVI than that in the arterial phase.

Previous studies indicated that a radiomics signature combined with clinical risk factors may be a viable substitute in the absence of a single reliable factor to predict LVI [13]. In this study, we combined the clinical risk factors with the radiomics signatures to construct a clinical-radiomics nomogram. Our study showed the clinical-radiomics nomograms achieved higher diagnostic performance than that of clinical model and radiomics model. Furthermore, DCA showed that the clinical-radiomics nomogram adds more benefit than either the radiomics model or clinical model for predicting LVI. For subgroup analyses, we found that the clinical-radiomics nomogram also showed higher AUC than that of clinical model and radiomics model both in T1-T2 stage and T3-T4 stage. Compared with T3-T4 stage, the sensitivity of CT for detecting LNM in T1-T2 stage was lower because the evaluation of lymph node status by CT images mainly relies on morphological features and most of the lymph node size in T1-T2 stage was normal [35,

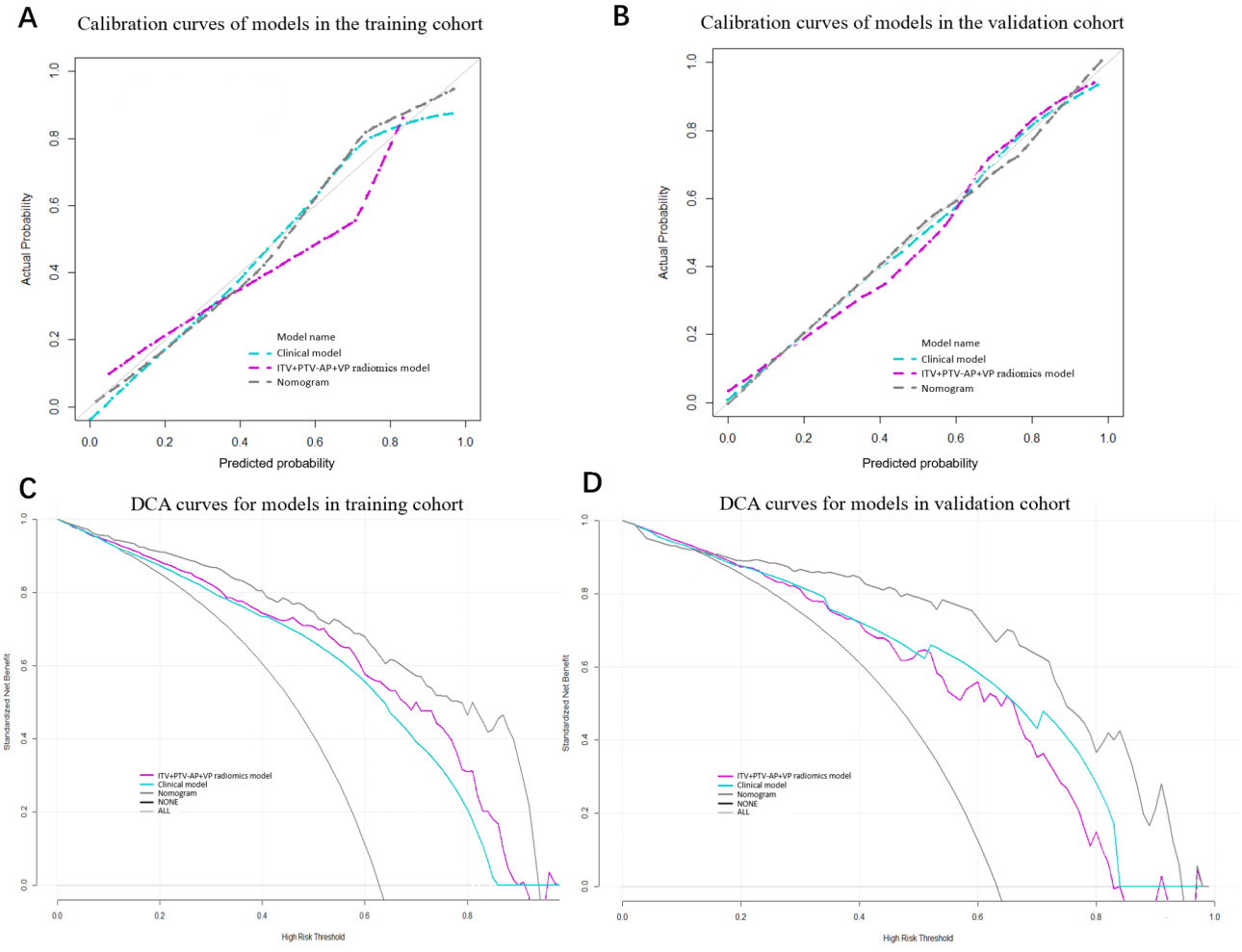

Fig. 5 The calibration curve of the combined model in the training cohort (**A**) and test cohort (**B**). The decision curve analysis curves of the three models in the training cohort (**C**) and test cohort (**D**) for predicting lymphovascular invasion (LVI)

Table 5 Subgroup analysis

Subgroup	Model	AUC(95%CI)	Sensitivity	Specificity
T1-2	ITV + PTV-AP + VP model	0.803(0.706-0.900)	1	0.019
	Clinical model	0.837(0.741–0.934)	0.903	0.415
	Nomogram	0.879(0.802–0.957)	1	0.019
T3-4	ITV + PTV-AP + VP model	0.828(0.770–0.885)	1	0.011
	Clinical model	0.756(0.691–0.821)	0.990	0.180
	Nomogram	0.883(0.886–0.929	1	0.011

CI: confidence intervals; AUC: the area under the receiver operating characteristic curve

36]. On the contrary, radiomics signature was not influenced by T staging and still maintained high sensitivity for predicting LNM [36]. Therefore, when combining clinical factors (AUC, 0.879 vs. 0.837) and radiomics features (AUC, 0.879 vs. 0.803) further improved the diagnostic performance because they are not completely identical and could complement each other.

There are several limitations in this study. Firstly, the potential observers' variation concerning both pathological and radiological could not be ignored despite we have developed a detailed measurement and evaluation process. In the future, multi-center collaborative research is needed to obtain larger data support and improve the reliability and universality of research. Secondly, this study only included arterial phase CT and venous phase CT-based radiomics analysis, while delay phase CT was not included. Third, the medical images were acquired with different machines and parameters that could affect radiomics features. However, in clinical practice, different protocols are performed in different centers, and this

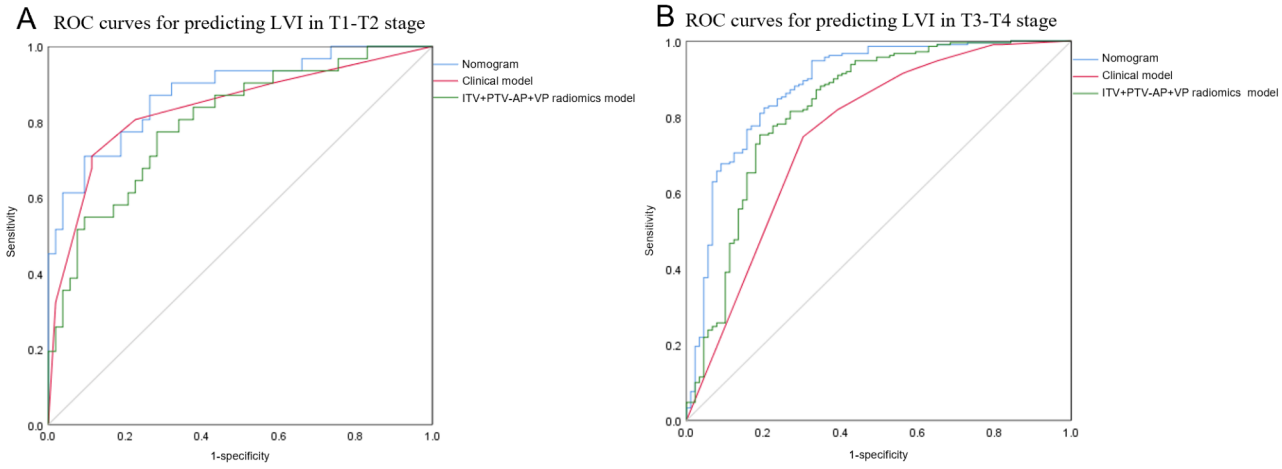

Fig. 6 Receiver operating characteristic (ROC) curves of radiomics model, clinical model, and clinical-radiomics nomogram for predicting LVI in T1-T2 stage (**A**) and T3-T4 stage (**B**) of gastric cancer

can in turn improve reproducibility in the multicenter studies.

Conclusion

In conclusion, our study suggests a clinical-radiomics nomogram that combining dual-phase contrast-enhanced CT-based intratumoral and peritumoral radscore, tumor differentiation status, CT-LNM, and CT-TNM staging achieved good prediction performance for preoperative predicting LVI. This preoperative assessment would aid in selecting a personalized treatment plan, such as neoadjuvant therapy, and evaluating the prognosis.

Abbreviations

AIC	Akaike information criterion
AJCC	American Joint Committee on Cancer
AP	Arterial phase
AUC	Areas under the receiver operating characteristic curve
CA19-9	Carbohydrate antigen 19 – 9
CEA	Carcinoembryonic antigen
CI	Confidence interval
CT	Computed tomography
DCA	Decision curve analysis
ICC	Intraclass correlation coefficient
LNM	Lymph node metastasis
LVI	Lymphovascular invasion
ROC	Receiver operating characteristic
VP	Venous phase

Supplementary Information

The online version contains supplementary material available at https://doi.org/10.1186/s12880-025-01569-5.

Supplementary Material 1

Acknowledgements

We sincerely appreciate all the individuals who participated in this study.

Author contributions

All authors contributed to the study's conception and design. Yun-hui Zhou: Conceptualization, Data curation, Formal analysis, Investigation, Methodology, Software, Validation, Visualization, Roles/Writing - original draft. Yang Liu: Conceptualization, Data curation, Investigation, Methodology, Resources, Validation, Visualization, Writing - original draft. Xin Zhang: Data curation, Software, Methodology, Visualization. Hong Pu: Conceptualization, Data curation, Funding acquisition, Methodology, Resources, Software, Validation, Visualization, Writing - review & editing. Hang Li: Conceptualization, Data curation, Formal analysis, Funding acquisition, Investigation, Methodology, Resources, Software, Validation, Visualization, Writing - review & editing. All authors commented on previous versions of the manuscript. All authors read and approved the final manuscript.

Funding

This work was supported by the Key Research Project of Sichuan Province (grant number, No.2022YFS0249) and China International Medical Exchange Foundation SKY Image Research Fund Development Project (Z-2014-07-1912).

Data availability

The data that support the findings of this study are not openly available due to reasons of sensitivity and are available from the corresponding author upon reasonable request. Data is located in data storage at Department of Radiology of Sichuan Academy of Medical Sciences and Sichuan Provincial People's Hospital.

Declarations

Ethics approval and consent to participate

The design and protocol of this retrospective study were approved by the Ethics Committee of Sichuan Provincial People's Hospital (No.2021086), and requirement to obtain written informed consent was waived because of the retrospective nature of the study. All methods in the study were carried out in accordance with the Helsinki guidelines and declaration.

Consent for publication

Not applicable.

Competing interests

The authors declare no competing interests.

Author details

[1]Department of Radiology, Sichuan Academy of Medical Sciences and Sichuan Provincial People's Hospital, 32# Second Section of First Ring Road, Qingyang District, Chengdu, Sichuan 610070, China
[2]Pharmaceutical Diagnostic Team, GE Healthcare, Beijing 100176, China

Received: 20 June 2024 / Accepted: 22 January 2025
Published online: 10 February 2025

References

1. Smyth EC, Nilsson M, Grabsch HI, Grieken NCV, Lordick F. Gastric cancer. Lancet. 2020;396(10251):635e48.
2. Sung H, Ferlay J, Siegel RL, Laversanne M, Soerjomataram I, Jemal A, et al. Global cancer statistics 2020: GLOBOCAN estimates of incidence and mortality worldwide for 36 cancers in 185 countries. CA Cancer J Clin. 2021;71(3):209–49.
3. Mei D, Zhao B, Zhang J, Luo R, Lu H, Xu H, et al. Impact of lymphovascular invasion on survival outcome in patients with gastric cancer. Am J Clin Pathol. 2020;153(6):833–41.
4. Fujikawa H, Koumori K, Watanabe H, Kano K, Shimoda Y, Aoyama T, et al. The clinical significance of lymphovascular invasion in gastric cancer. Vivo (Brooklyn). 2020;34(3):1533–9.
5. Choi S, Song JH, Lee S, Cho M, Kim YM, Kim HL, et al. Lymphovascular invasion: traditional but vital and sensible prognostic factor in early gastric cancer. Ann Surg Oncol. 2021;28(13):8928–35.
6. Zhang CD, Ning FL, Zeng XT, Zeng XT, Dai DQ. Lymphovascular invasion as a predictor for lymph node metastasis and a prognostic factor in gastric cancer patients under 70 years of age: a retrospective analysis. Int J Surg. 2018;53:214–20.
7. Hirabayashi S, Kosugi S, Isobe Y, Nashimoto A, Oda I, Hayashi K, et al. Development and external validation of a nomogram for overall survival after curative resection in serosa-negative, locally advanced gastric cancer. Ann Oncol. 2014;25:1179–84.
8. Ma ZL, Liang CH, Huang YQ, He L, Liang CS, Chen X, et al. Can lymphovascular invasion be predicted by preoperative multiphasic dynamic CT in patients with advanced gastric cancer? Eur Radiol. 2017;27(8):3383–91.
9. Li J, Xu S, Wang Y, Fang M, Ma F, Xu C, et al. Spectral CT-based nomogram for preoperative prediction of perineural invasion in locally advanced gastric cancer: a prospective study. Eur Radiol. 2023;33(7):5172–83.
10. Wang XX, Ding Y, Wang SW, Dong D, Li HL, Chen J, et al. Intratumoral and peritumoral radiomics analysis for preoperative Lauren classification in gastric cancer. Cancer Imaging. 2020;20(1):83.
11. Huang W, Jiang Y, Xiong W, Sun ZP, Chen CL, Yuan QY, et al. Noninvasive imaging of the tumor immune microenvironment correlates with response to immunotherapy in gastric cancer. Nat Commun. 2022;13(1):5095.
12. Jiang Y, Wang H, Wu J, Chen C, Yuan Q, Huang W, et al. Noninvasive imaging evaluation of tumor immune microenvironment to predict outcomes in gastric cancer. Ann Oncol. 2020;31(6):760–8.
13. Chen XF, Yang ZQ, Yang JD, Liao YT, Pang PP, Fan WX, et al. Radiomics analysis of contrast-enhanced CT predicts lymphovascular invasion and disease outcome in gastric cancer: a preliminary study. Cancer Imaging. 2020;20(1):24.
14. Hu YH, Xie CY, Yang H, Ho JWK, Wen J, Han LJ, et al. Assessment of intratumoral and peritumoral computed tomography radiomics for predicting pathological complete response to neoadjuvant chemoradiation in patients with esophageal squamous cell carcinoma. JAMA Netw Open. 2020;3(9):e2015927.
15. Ajani JA, In. In: Sano H T, editor. et al. AJCC Cancer Staging Manual. New York: eighth ed., Springer-; 2016.
16. Kim AY, Kim HJ, Ha HK. Gastric cancer by multidetector row CT: preoperative staging. Abdom Imaging. 2005;30:465–72.
17. Bosman FT, Carneiro F, Hruban RH, Theise ND. WHO classification of tumours of the digestive system. 4th ed. Geneva:World Health Organization; 2010.
18. Amin MB, Greene FL, Edge SB, Compton CC, Gershenwald JE, Brookland RK, et al. The eighth edition AJCC cancer staging manual: continuing to build a bridge from a population-based to a more personalized approach to cancer staging. CA Cancer J Clin. 2017;67:93–9.
19. Guo Q, Sun Q, Bian X, Wang M, Dong H, Yin H, et al. Development and validation of a multiphase CT radiomics nomogram for the preoperative prediction of lymphovascular invasion in patients with gastric cancer. Clin Radiol. 2023;78(8):e552–9.
20. Fan LJ, Li J, Zhang HL, Yin HK, Zhang RG, Zhang JB, et al. Machine learning analysis for the noninvasive prediction of lymphovascular invasion in gastric cancer using PET/CT and enhanced CT-based radiomics and clinical variables. Abdom Radiol (NY). 2020;47(4):1209–22.
21. Wang P, Chen K, Han Y, Zhao M, Abiyasi N, Peng H, et al. Prediction model based on radiomics and clinical features for preoperative lymphovascular invasion in gastric cancer patients. Future Oncol. 2023;19(23):1613–26.
22. He Y, Yang M, Hou R, Ai S, Nie T, Chen J, et al. Preoperative prediction of perineural invasion and lymphovascular invasion with CT radiomics in gastric cancer. Eur J Radiol Open. 2024;12:100550.
23. Li J, Yin HK, Zhang HL, Wang Y, Ma F, Li LM, et al. Preoperative risk stratification for gastric cancer: the establishment of dual-energy CT-based radiomics using prospective datasets at two centers. Acad Radiol. 2024;31(11):4466–77.
24. Li Q, Feng QX, Qi L, Liu C, Zhang J, Yang G, et al. Prognostic aspects of lymphovascular invasion in localized gastric cancer: new insights into the radiomics and deep transfer learning from contrast–enhanced CT imaging. Abdom Radiol (NY). 2022;47(2):496–507.
25. Wang XL, Fang JP, Tang RY, Chen XM. Different significance between intratumoral and peritumoral lymphatic vessel density in gastric cancer: a retrospective study of 123 cases. BMC Cancer. 2010;10:299.
26. Pak KH, Jo A, Choi HJ, Choi Y, Kim H, Cheong JH. The different role of intratumoral and peritumoral lymphangiogenesis in gastric cancer progression and prognosis. BMC Cancer. 2015;15:498.
27. Liu CC, Li LM, Chen XZ, Huang CC, Wang R, Liu YY, et al. Intratumoral and peritumoral radiomics predict pathological response after neoadjuvant chemotherapy against advanced gastric cancer. Insights Imaging. 2024;15(1):23.
28. Yardımcı AH, Koçak B, Bektaş CT, Sel İ, Yarıkkaya E, Dursun N, et al. Tubular gastric adenocarcinoma: machine learning-based CT texture analysis for predicting lymphovascular and perineural invasion. Diagn Interv Radiol. 2020;26(6):515–22.
29. Cao F, Hu YW, Li P, Liu Y, Wang K, Ma L, et al. Lymphangiogenic and angiogenic microvessel density in Chinese patients with gastric carcinoma: correlation with clinicopathologic parameters and prognosis. Asian Pac J Cancer Prev. 2013;14(8):4549–52.
30. Gao P, Zhou GY, Zhang QH, Su ZX, Zhang TG, Xiang L, et al. Lymphangiogenesis in gastric carcinoma correlates with prognosis. J Pathol. 2009;218(2):192–200.
31. Padera TP, Kadambi A, di Tomaso E, Carreira CM, Brown EB, Boucher Y, et al. Lymphatic metastasis in the absence of functional intratumor lymphatics. Science. 2002;296(5574):1883–6.
32. Komori M, Asayama Y, Fujita N, Fujita N, Hiraka K, Tsurumaru D, et al. Extent of arterial tumor enhancement measured with preoperative MDCT gastrography is a prognostic factor in advanced gastric cancer after curative resection. AJR Am J Roentgenol. 2013;201(2):W253–61.
33. Tsurumaru D, Miyasaka M, Muraki T, Asayama Y, Nishie A, Oki E, et al. Diffuse-type gastric cancer: specific enhancement pattern on multiphasic contrast-enhanced computed tomography. Jpn J Radiol. 2017;35(6):289–95.
34. Liu SL, Liu S, Ji CF, Zheng HH, Pan X, Zhang YJ, et al. Application of CT texture analysis in predicting histopathological characteristics of gastric cancers. Eur Radiol. 2017;27(12):4951–9.
35. Dong ZB, Xiang HT, Wu HM, Cai XL, Chen ZW, Chen SS, et al. LncRNA expression signature identifed using genome–wide transcriptomic profling to predict lymph node metastasis in patients with stage T1 and T2 gastric cancer. Gastric Cancer. 2023;26(6):947–57.
36. Gao XJ, Ma T, Cui J, Zhang Y, Wang L, Li H, et al. A radiomics-based model for prediction of lymph node metastasis in gastric cancer. Eur J Radiol. 2020;129:109069.

Publisher's note